A gradient method for the quantitative analysis of cell movement and tissue flow and its application to the analysis of multicellular *Dictyostelium* development

Florian Siegert[1], Cornelis J. Weijer[1],*, Atsushi Nomura[2] and Hidetoshi Miike[2]

[1]Zoologisches Institut, Universität München, Luisenstr. 14, 80333 München, FRG
[2]Department of Electrical and Electronic Engineering, Yamaguchi University, Tokiwadai 2557, Ube, 755 Japan

*Author for correspondence

SUMMARY

We describe the application of a novel image processing method, which allows quantitative analysis of cell and tissue movement in a series of digitized video images. The result is a vector velocity field showing average direction and velocity of movement for every pixel in the frame. We apply this method to the analysis of cell movement during different stages of the *Dictyostelium* developmental cycle. We analysed time-lapse video recordings of cell movement in single cells, mounds and slugs. The program can correctly assess the speed and direction of movement of either unlabelled or labelled cells in a time series of video images depending on the illumination conditions.

Our analysis of cell movement during multicellar development shows that the entire morphogenesis of *Dictyostelium* is characterized by rotational cell movement. The analysis of cell and tissue movement by the velocity field method should be applicable to the analysis of morphogenetic processes in other systems such as gastrulation and neurulation in vertebrate embryos.

Key words: cell movement, velocity vector field, morphogenesis, chemotaxis, digital image processing, *Dictyostelium discoideum*

INTRODUCTION

During morphogenesis individual cells are organized into distinct and well-defined tissues and organs. This requires a complex and coordinated series of cellular movements and intensive communication between the cells. Due to its remarkable life cycle the cellular slime mould *Dictyostelium discoideum* is exceptionally well suited for the study of the process of spatio-temporal pattern formation. The life cycle of *Dictyostelium* is divided into distinct phases - one in which the cells live as solitary amoebae and multiply by cell division and one in which the single cells aggregate chemotactically and form a multicellular organism. Depletion of nutrients initiates the developmental program, which ultimately leads to a fruiting body consisting of a stalk carrying a spore head.

Multicellular morphogenesis is the result of differential cell movement of the various cell types in the multicellular aggregate and slug. There is increasing evidence that periodic signals and chemotaxis not only control the early aggregation phase (Alcantara and Monk, 1974; Wessels et al., 1992) but also organize cell movement and differentiation during multicellular development (Durston and Vork, 1979; Siegert and Weijer, 1992a). During early aggregation cell movement and behaviour of single cells have been investigated in a quantitative way using a variety of methods (Varnum et al., 1985;

Segall, 1988; Fisher et al., 1989; Steinbock et al., 1991; Wessels et al., 1992),. Only a few studies have attempted to quantitatively measure cell movement in the multicelluar stages of development. Up to now most cell tracking experiments of individual labelled cells in aggregation streams and slugs show that the cells go through periodic velocity and shape changes, which indicates that the cells move in a chemotatic fashion (Durston and Vork, 1979; Condeelis et al., 1990; Siegert and Weijer, 1991, 1992a,b; Segall, 1992).

In order to understand *Dictyostelium* morphogenesis it is necessary to investigate the behaviour of many cells simultaneously (Clark and Steck, 1979; Durston and Vork, 1979; Bonner et al., 1989). All measurements performed till now required either fluorescent labelling of the cells or labelling with the vital dye neutral red. A restriction of both methods is that only subpopulations of cells can be measured. It would be desirable to analyse the behaviour of every cell in a multicellular structure at every stage during multicellular development. Furthermore, most cell tracking methods rely on the visual identification of cells, combined with manual tracking, which is very tedious. Often it is not possible to positively identify the same cell in successive video frames.

To resolve these problems we adapted a program, which was developed to investigate the flow of particles in fluids (Nomura et al., 1991), to measure cell movement in multicellular stages

of *Dictyostelium* development. This program calculates the average velocity vector for every pixel in a time series of digitized video images. With this method it is not necessary to identify single cells in order to measure cell movement. The velocity of virtually all optically distinct structures, e.g. intracellular vacuoles, nuclei and vesicles that move, can be detected. This method allowed us to quantitatively analyse direction and velocity of tissue movement in multicellular stages, in which single unlabelled cells cannot be identified unambiguously. Our results strongly confirm the hypothesis that the whole morphogenesis of *Dictyostelium* is brought about by orbital cell movement (Clark and Steck, 1979; Siegert and Weijer, 1992a).

MATERIALS AND METHODS

Strains and developmental conditions

All experiments were performed with axenic AX-2 or AX-3 cells grown according to standard culture conditions (Sussmann, 1987). To initiate development axenically grown cells were washed twice in KK2 (20 mM potassium phosphate buffer, pH 6.8). Slugs were obtained by placing drops of cells (10^8/ml), washed once in distilled water, on 1% water agar plates (1% Difco Bacto agar in distilled water). The plates were then incubated in the dark for 24-48 hours at 18°C. To obtain aggregation fields, streams and mounds the cells were washed twice in KK2 and resuspended in KK2 at a density of 5×10^6cells/ml. Samples (5 ml) of the cell suspension (2.5×10^7cells) were poured on 1% KK2 buffer agar plates. After 5-10 minutes the cells settled on the agar and the supernatant was poured off. After 4-6 hours of development aggregation streams formed and, after 8 hours, mounds. In some cases the cells were labelled with the vital dye neutral red by incubating the washed cells in 0.06% neutral red in KK2 for 5 minutes, followed by a wash in KK2.

Video microscopy

Video films of the different developmental stages were made by placing Petri dishes with developing cells on agar on a Zeiss IM 35 inverted microscope equipped with objectives of different magnifications (×16, ×32, ×40). The objective was slightly heated (2 deg. C above the room temperature) to avoid condensation. Video films were made with a Hamamatsu C-2400 Silicon Intensified Target (SIT) camera adjusted to half-maximal sensitivity to reduce illumination intensity. Slugs were filmed while migrating under mineral oil as described earlier (Siegert and Weijer, 1992a).

Digital image processing

Digital image processing was performed with a Tandon AT compatible computer equipped with an Imaging Technology FG 100 board (resolution 512×512 pixel). In several experiments noise was reduced by averaging 10 video images in real time (25 frames/second) before storing on a Sony EVT-801CE time-lapse video recorder. The calculations and the display of the vector fields were performed with an IBM compatible 486 computer equipped with an Imaging Technology AFG board.

Calculation of velocity vector fields

The velocity vector at each pixel on an image plane is calculated by the modified gradient method of Nomura et al. (1991). The following equation is the basic constraint of the gradient-based method:

$$\frac{\partial f}{\partial t} + \frac{\partial f}{\partial x} v_x + \frac{\partial f}{\partial y} v_y = 0, \tag{1}$$

where $f(x,y,t)$ is the spatio-temporal brightness distribution of an

image sequence and $v=(v_x,v_y)$ is a velocity vector at (x,y,t). $\partial f/\partial t$, $\partial f/\partial x$ and $\partial f/\partial y$ are computed from the digitized brightness distribution $f(x,y,t)$ as follows:

$$\frac{\partial f}{\partial t} \approx \left[\sum_{i=-1}^{1} \sum_{j=-1}^{1} \{f(x+i,y+j,t+1)-f(x+i,y+j,t-1)\}/2 \right]/9 \tag{2}$$

$$\frac{\partial f}{\partial x} \approx \left[\sum_{j=-1}^{1} \sum_{k=-1}^{1} \{f(x+1,y+j,t+k)-f(x-1,y+j,t+k)\}/2 \right]/9 \tag{3}$$

$$\frac{\partial f}{\partial y} \approx \left[\sum_{i=-1}^{1} \sum_{k=-1}^{1} \{f(x+i,y+1,t+k)-f(x+i,y-1,t+k)\}/2 \right]/9. \tag{4}$$

The velocity vector cannot be computed locally, since we have only one constraint equation (1) at each pixel and in each frame, while a velocity vector has two unknowns: v_x and v_y. Additional constraints have to be introduced. Some references have assumptions on the instantaneous velocity fields such as spatial smoothness constraint (Horn and Schunck, 1981) and spatial constancy in a small neighbourhood (Kearney et al., 1987) in the velocity vector field. Here we assume a temporal stationarity of the velocity field:

$$\frac{\partial v}{\partial t} = 0. \tag{5}$$

For consecutive image frames with a stationary velocity field we can expect to obtain a high-accuracy velocity field with fine spatial resolution by the above assumption, even though the images are polluted by noise. If the assumption is satisfied from $t=0$ to $t=T$, we can define the following error function at (x,y).

$$E(x,y) = \sum_{t=0}^{T} \left\{ \frac{\partial f}{\partial t} + \frac{\partial f}{\partial x} v_x(x,y) + \frac{\partial f}{\partial y} v_y(x,y) \right\}^2. \tag{6}$$

The velocity vector $v(x,y)$ is obtained by the least squares method minimizing equation (6) with respect to $v_x(x,y)$ and $v_y(x,y)$. That is the following two equations are obtained by $\partial E(x,y)/\partial v_x(x,y)=0$ and $\partial E(x,y)/\partial v_y(x,y)=0$:

$$\frac{\partial E(x,y)}{\partial v_x(x,y)} = 2\sum_{t=0}^{T} \left\{ \frac{\partial f}{\partial t} + \frac{\partial f}{\partial x} v_x(x,y) + \frac{\partial f}{\partial y} v_y(x,y) \right\} \frac{\partial f}{\partial x} = 0 \tag{7}$$

$$\frac{\partial E(x,y)}{\partial v_y(x,y)} = 2\sum_{t=0}^{T} \left\{ \frac{\partial f}{\partial t} + \frac{\partial f}{\partial x} v_x(x,y) + \frac{\partial f}{\partial y} v_y(x,y) \right\} \frac{\partial f}{\partial y} = 0. \tag{8}$$

By solving the simultaneous equations (7) and (8) we finally obtain the velocity vector $v=(v_x(x,y),v_y(x,y))$ as follows:

$$v_x(x,y) =$$
$$-\frac{1}{\Delta} \left\{ \sum_{t=0}^{T} \left(\frac{\partial f}{\partial y}\right)^2 \sum_{t=0}^{T} \left(\frac{\partial f}{\partial x}\frac{\partial f}{\partial t}\right) - \sum_{t=0}^{T} \left(\frac{\partial f}{\partial x}\frac{\partial f}{\partial t}\right) \sum_{t=0}^{T} \left(\frac{\partial f}{\partial y}\frac{\partial f}{\partial t}\right) \right\} \tag{9}$$

$$v_y(x,y) =$$
$$-\frac{1}{\Delta} \left\{ -\sum_{t=0}^{T} \left(\frac{\partial f}{\partial x}\frac{\partial f}{\partial y}\right) \sum_{t=0}^{T} \left(\frac{\partial f}{\partial x}\frac{\partial f}{\partial t}\right) + \sum_{t=0}^{T} \left(\frac{\partial f}{\partial x}\right)^2 \sum_{t=0}^{T} \left(\frac{\partial f}{\partial x}\frac{\partial f}{\partial t}\right) \right\}, \tag{10}$$

where

$$\Delta = \sum_{t=0}^{T}\left(\frac{\partial f}{\partial x}\right)^2 \sum_{t=0}^{T}\left(\frac{\partial f}{\partial y}\right)^2 - \left\{\sum_{t=0}^{T}\left(\frac{\partial f}{\partial x}\,\frac{\partial f}{\partial y}\right)\right\}^2 \;. \qquad (11)$$

By applying equations (9), (10) and (11) to each pixel of an image sequence we can evaluate the velocity field.

The algorithm was used to calculate the average movement over a sequence of 16 consecutive digitized video images (256x256 pixel maximal size). The program was written in C (Microsoft C/C++ 7.0) and runs on an IBM AT-compatible 486 computer (33 MHz) equipped with 20 MB RAM memory. Calculation of the velocity vector field for one complete sequence takes around 45 seconds of cpu time. After calculation of the velocity field values, the result can be displayed as a vector field in the 8 bit overlay of an image processing board (AFG board, Imaging Technology) or printed on a laser printer. The AFG board allows the simultaneous display of the video sequence and the calculated vector field.

The origin of each vector is indicated by a dot or a half-circle and the length of the vector encodes the velocity at that pixel. Long vectors indicate fast movement and short vectors slow movement. The length of the vectors is plotted in arbitrary units so as to give a good visual impression of both magnitude and direction. Additionally the velocity can be color coded to visualize small differences in movement speed in various regions of the multicellular structure. Real-time averaging before storing the video frame on a time-lapse recorder reduced noise and enhanced the quality of the calculated velocity fields significantly. For every pixel in the image a velocity is calculated. In order to reduce noise even further 4-16 vectors were averaged.

RESULTS

Chemotactic cell movement of single cells

In order to test the performance of the gradient velocity field analysis method on a biological object we measured the movement of single cells migrating on agar. Axenic cells were washed and placed on KK2 agar at a density of 10^6 cells/plate. After 3-4 hours the cells were aggregation competent and started to move intensively. Moving cells were filmed and recorded with a time-lapse video recorder. Sequences suitable for the velocity analysis were chosen from these films. Data files of 16 consecutive digitized video images taken at 5-second intervals were used as input for the vector analysis program. Fig. 1A-C shows a sequence of three consecutive time points in which a single cell moves in a diagonal downward direction. The graphical overlay of the digitzed video images displays the velocity vector field calculated over this time series. To reduce noise 25 vectors were averaged and are displayed as a single vector in Fig. 1A-C. The vector field clearly indicates the track of the cell. The length of the vectors is proportional to the velocity that was detected at this location in the cell. Black half-circles indicate the starting point of each vector and thereby the direction of movement. Some movement is detected outside of the cell, as indicated by randomly oriented very short vectors. This can by attributed to noise in the video signal between the successive video frames. Fig. 1D displays the average velocity for each pixel in the image sequence. The velocity of each vector is colour coded: black indicates slow, and white fast, movement.

To calculate the rate of cell movement all vectors above noise were averaged. The analysis shows that this cell moves with a speed of 9 μm/min, which agrees with previous measurements (Varnum et al., 1985; Fisher et al., 1989; Siegert and Weijer, 1992b). These experiments (n=10) confirmed that both velocity and direction of movement are determined correctly by the vector analysis program. The method also allows the determination of relative rates of cell movement in different parts of the cell. In Fig. 1D the movement of extending and retracting pseudopods can be seen as bright white areas, which indicate high velocities. The analysis of subsets of vectors allows determination of velocities in different parts of the cell. In Fig. 1C three squares indicate different regions within the cell in which the velocities were determined. Analysis of the vectors belonging to a extending pseudopod (lower square) show that the pseudopod extends with a velocity of 10.2 μm/min. Retraction of the rear end of the cell (upper square) occurs at 11.7 μm/min while the movement of the central body of the cell (middle square) occurs at 6.2 μm/min.

The validity of the vector method has previously been tested on the analysis of computer-generated objects, which moved in known direction and with a known speed (Nomura et al., 1991). It has been shown to perform well with such artificial objects. We performed the velocity analysis of single cells to validate the method on a biological object. The results clearly show that this method is very well suited to quantitatively analyse the dynamics of amoeboid cell movement.

Cell movement in mounds

During the aggregation process cells move towards the aggregation center. In aggregation streams and centers unlabelled single cells cannot be identified unless they are labelled by fluorescent marker molecules. We analysed cell movement in late aggregates and mounds. Fig. 2 shows a typical example of the analysis of cell movement in a mound of strain AX-3. Some cells are still entering the aggregate in a stream in the top left corner; individual cells cannot easily be identified (Fig. 2A). The velocity field analysis of 16 consecutive images shows that cells in the aggregate body move on circular orbits around a central core (Fig 2B,D). The length and the colour of the vectors indicate the velocity: long yellow vectors indicate fast, and short dark red vectors indicate slow, movement. In strain AX-3 we observed rotational cell movement in all experiments (n>30). Fig. 2C displays the corresponding velocity for each pixel in the image sequence. The velocity of each vector is colour coded: red indicates slow, and blue fast, movement. Cells in the periphery of the mound move considerably faster than cells in the core and in the aggregation stream (Fig. 2C,D). The quantitative analysis of these observations is displayed in Fig. 2E,F. Fig. 2E shows the averaged velocities along a cross-section of the image through the aggregation stream. The velocity profile across a section through the center of the aggregate is displayed in Fig. 2F. Cells in the aggregation stream move with an average velocity of 10 μm/min while rotating cells in the mound move with a maximum speed of 20 μm/min. This increase in overall cell movement speed during *Dictyostelium* development corresponds with previous measurements (Durston and Vork, 1979; Siegert and Weijer, 1992b). Cells in the centre of the mound show a reduced cell movement velocity (Fig. 2F). These data are in agreement with recently published qualitative observations of rotational cell movement in mounds of strain AX-3 (Elliot et al., 1993).
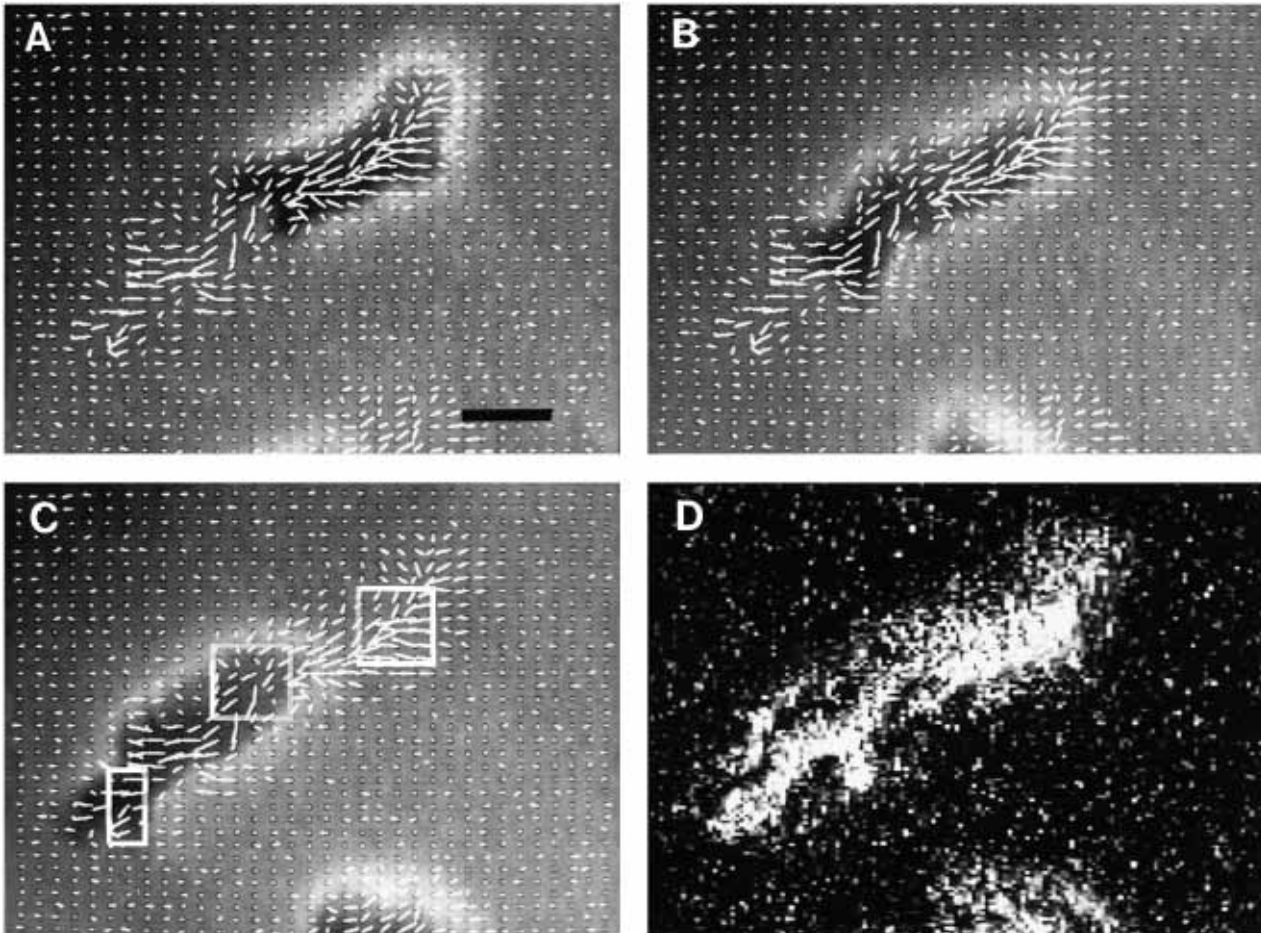
Fig. 1. Vector field analysis of the movement of a single cell. (A,B,C) A sequence of phase-contrast micrographs of a single cell migrating in an aggregation field of strain AX-2 with its corresponding velocity vector field (160×160 pixels). The velocity vector field was calculated from a series of 16 consecutive video frames taken at 5-second time intervals. The same vector field is superimposed on three different digitized video images of the time series (A, 0 seconds; B, 40 seconds; C, 80 seconds) that were used to calculate the vector field. The length of the vectors indicates the velocity of movement in arbitrary units. The vectors shown are averaged over 25 pixels. In (C) three different regions are indicated by white squares in which local velocities of retracting and extending pseudopods and the main cell body were determined. (D) Velocity for each pixel in the image sequence. The velocity of each vector is colour coded: black indicates slow, and white fast, movement. Bar, 10 μm.

Cell movement of prestalk and anterior-like cells in slugs

The next stage in the development of *Dictyostelium* is the formation of the migratory slug. The first sign of slug formation is the formation of a tip on top of the aggregate, which directs all further morphogenesis. Earlier experiments suggested that periodic signals emitted by the tip coordinate the movement of the individual cells in slugs (Rubin and Robertson, 1975; Siegert and Weijer, 1991). In a previous investigation we showed that neutral red-stained prestalk cells in the slug tip rotate along the long axis of the slug, while the anterior-like cells in the prespore zone of the slug move forward in the direction of slug migration. The analysis was performed by an interactive tracking method, which was based on the visual identification of labelled cells (Siegert & Weijer, 1992a).

To investigate overall movement of all neutral red-stained cells in migrating slugs, cells were labelled with the vital dye neutral red and placed under mineral oil as described by Siegert

and Weijer (1992a). Neutral red stains prestalk and anterior-like cells while prespore cells appear unstained in transmitted light. Fig. 3A-D shows the front 40% of a slug. The slug moves from left to right. The prestalk zone of the slug is characterized by its dark appearance due to the intense staining of vacuoles, which appear as black dots in the photograph in Fig. 3A. Anterior-like cells, which represent 5-10% of all cells in a slug, are dispersed in the unstained prespore zone. The velocity field analysis shows that prestalk and anterior-like cells move along different trajectories. Fig. 3B shows the calculated velocity field, each vector displays the averaged velocity of 36 pixels. The direction of the vectors shows that anterior-like cells in the prespore zone move in the direction of slug migration, while prestalk cells in the posterior prestalk zone move at an angle upward to the direction of slug migration. Prestalk cells in the most anterior prestalk zone move at an angle downward with respect to the direction of slug migration. In Fig. 3C more vectors are shown, each vector displays the average of 9 pixels. This representation gives a
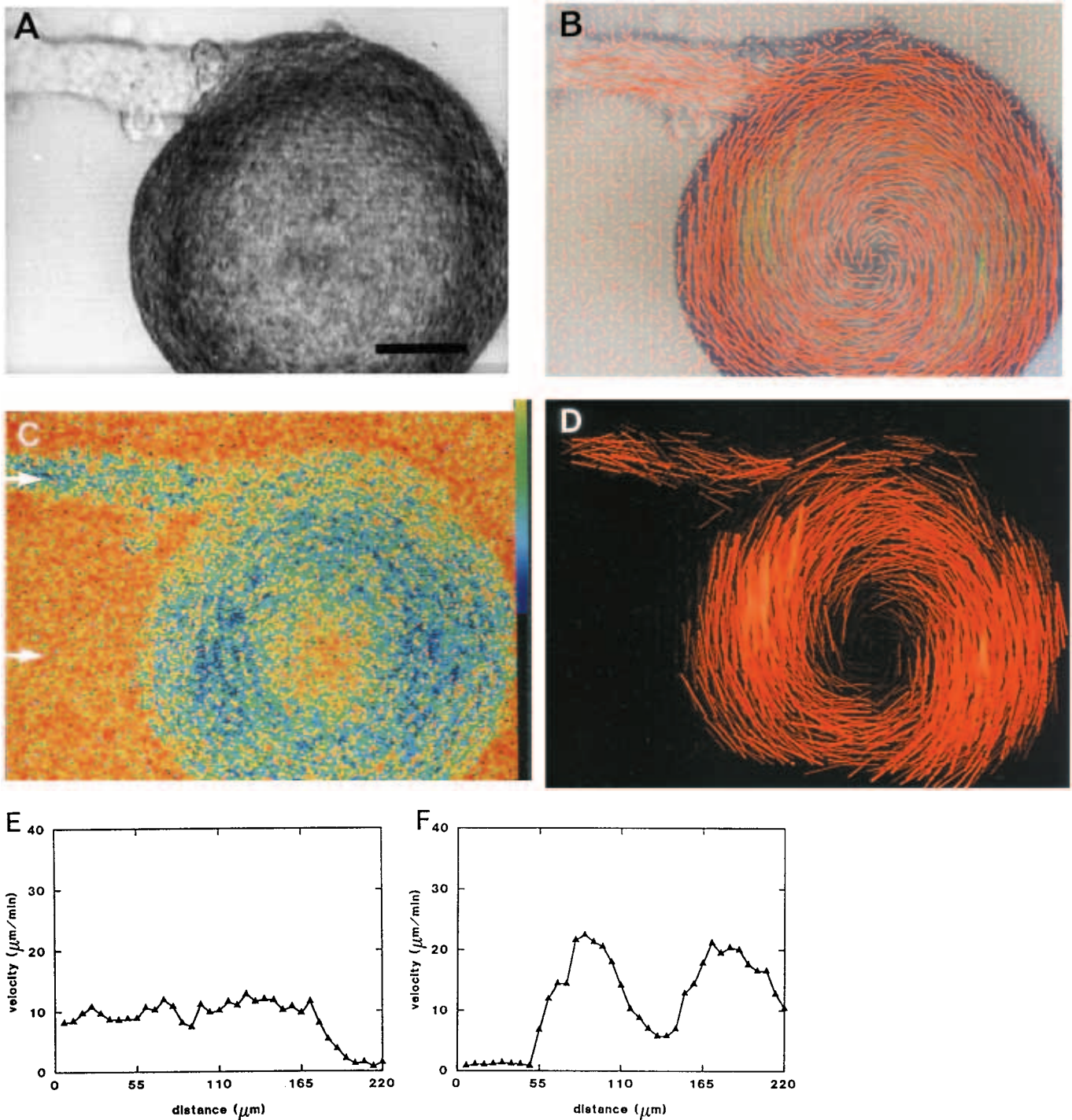
Fig. 2. Analysis of cell movement in a mound of strain AX-3. (A) Photograph of a mound of AX3 with a stream of cells entering the mound (top left). (B) Overlay of the picture shown in (A) and its velocity vector field calculated from 16 consecutive video frames (220×220 pixel) taken at 5-second time intervals. The velocity is colour coded: red represents slow, and yellow fast, movement. The vectors shown are averaged over 16 pixels. (C) Velocity for each pixel in the image sequence. The velocity is colour coded: red represents slow, and blue fast, movement. (D) Same velocity vector field as in (B), but different colour coding of the velocity vectors: slow movement (short vectors) are black; fast movement (long vectors) are red. (E and F) Velocity profiles across the mound in a horizontal direction (upper and lower arrows in (C)). Each data point represents the average of 48 velocity values (6×8 pixel). Bar, 50 μm.

better impression of the local dynamics of cell movement. The vectors radiating from the slug tip indicate the forward movement of the slug during the measurement.

By plotting the average velocity at every pixel as a grey value from black (low velocity) to white (high velocity) it becomes clear that the dark neutral red-stained vacuoles are
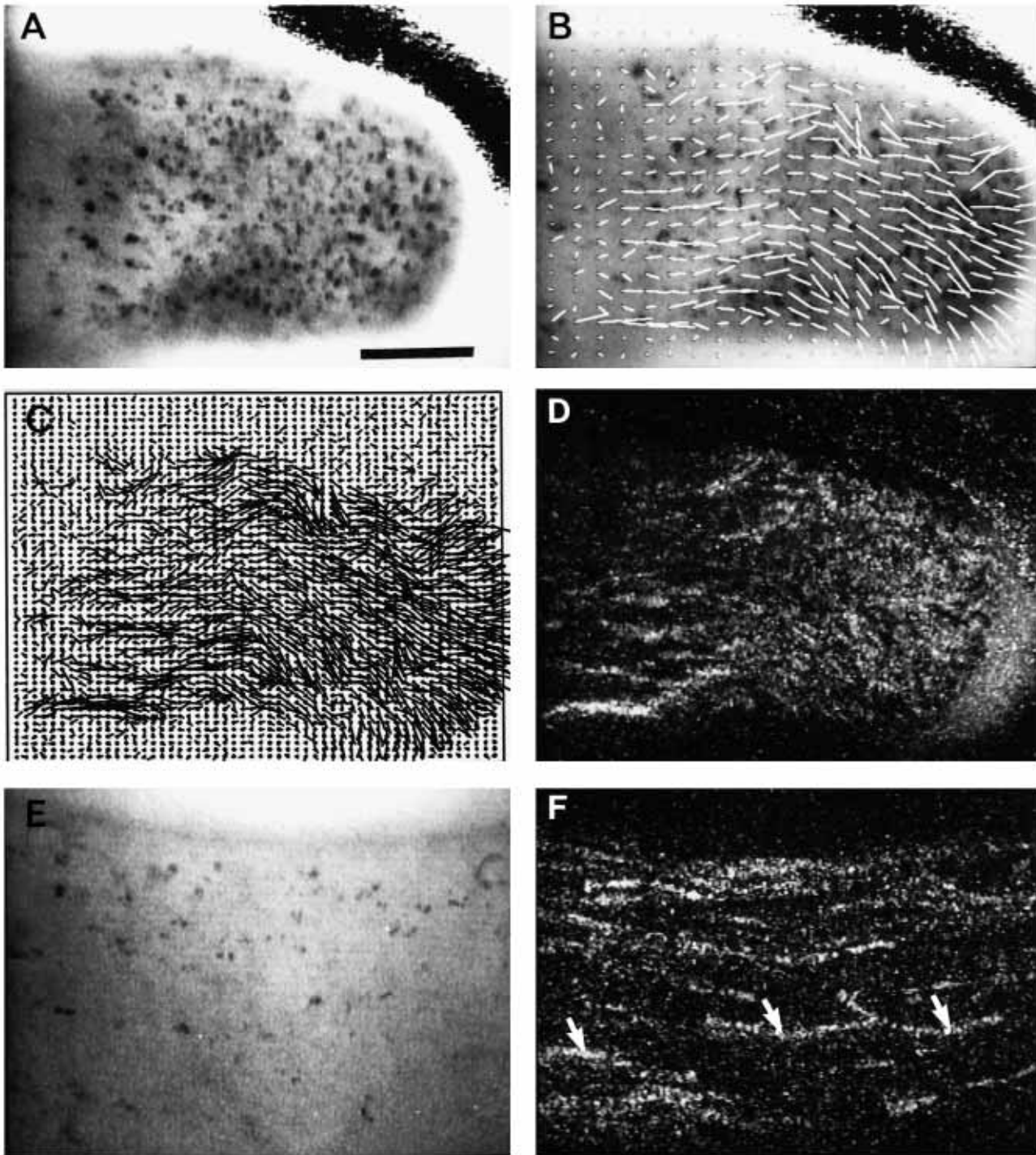
Fig. 3. Movement analysis in a migrating AX-2 slug. (A) Photograph of the front 40% of a neutral red-stained slug. (B) Velocity vector field for the slug shown in (A) for 16 consecutive video frames (220×220 pixel) taken at 5-second time intervals. The vectors shown are averaged over 36 pixels. (C) Same velocity vector field as in (B) but only 9 vectors are averaged. (D) Velocity distribution for all pixels in the image sequence. The velocity of each vector colour coded: black indicates slow, and white fast, movement. (E) Photograph of the middle part of a neutral red-stained slug. (F) The average velocity of each pixel in the time series is shown in a grey scale going from white (50 μm/min) to black (0 μm/min). The tracks of three neutral red-stained anterior-like cells are indicated by white arrows. Bar, 50 μm.

tracked over time accurately (compare Fig. 3A and D). Fig. 3E shows a contrast-enhanced video image of the middle part of a slug. The stained vacuoles belong to anterior-like cells that are dispersed in the prespore zone of slugs. The velocity field

analysis (Fig. 3F) shows clearly that anterior-like cells move straight forward in direction of slug movement.

In order to check whether the rate of particle movement as detected by the vector analysis is correct we determined the

velocity of selected neutral red-stained particles and compared these values with results obtained by interactive tracking of the same particles. To determine the average velocity of a particle by the vector method we first determined all vector values belonging to a particle track by interactively setting a threshold. Then the velocities of all vectors above this threshold were averaged. The velocities of the three particles indicated by white arrows in Fig. 3F are 23.4, 27.8 and 29.8 μm/min (left to right). These measurements can be compared directly with values obtained by interactive tracking: the velocities of these particles (22.6, 27.4 and 26.8 μm/min, left to right) differ by only 5%. Both methods gave similar results in this and other experiments (n=5), within the error of the experiment.

These results show that our present findings, for both the direction and the velocity of movement, are in absolute agreement with our previous observations on selected neutral red-stained cells. However, the velocity field analysis allows determination of movement of all particles in a field simultaneously and is much faster to perform.

DISCUSSION

Establishment of a pixel-based method to analyse cell movement

We investigated the ability of a pixel-based gradient method to analyse complex cell and tissue movements in different developmental stages of the slime mould *Dictyostelium discoideum*. We calibrated the velocity analysis on the movement of single cells (Fig. 1) and showed that at high magnifications it is possible to follow the expansion and retraction of pseudopods. In cases where single cells cannot be identified individually this method allows a quantitative analysis of tissue flow (Fig. 2). The method has proven to be especially powerful in determining tissue movements in the absence of clearly detectable cell boundaries. It is also possible to track the movement of labelled cells or particles and vesicles within cells in multicellular aggregates (Fig. 3).

The vector method determines the movement of all distinct grey value structures in a sequence of video images over time. By choosing the appropriate magnification, lighting conditions and time scale this method can be used to analyse very different biological objects ranging from intracellular organelles to tissue movement in embryos.

We verified the usefulness of this method on single cells and tissue movement in multicellular aggregates, that differ in size by 30-fold. In both cases the results of the vector analysis compared well with values obtained with other methods. At a higher magification (×1000) and different optical conditions (Nomarski optics) this method would be able to measure intracellular particle transport and cytoplasmatic flow.

Since the vector method detects the movement of grey value patterns lighting conditions have a strong influence on which objects are detected. In mounds individual cells and cell boundaries cannot be identified (Fig. 2). For these measurements we have therefore chosen lighting conditions that enhance the visibility of intracellular structures leading to a distinct grey value pattern for each cell, which covered more than 20 pixels on average. The vector method allowed the quantitative determination of tissue flow in different parts of the mound (Fig. 2E,F). This information would be very

difficult to obtain by interactive tracking methods, since it is almost impossible to recognize individual cells by eye in successive images. We have shown that cells in the center move more slowly than the cells at the periphery. Furthermore, cells that enter the aggregation stream move more slowly than the cells in the aggregate. This level of resolution in the analysis of cell movement in unstained multicellular structures was impossible to obtain until now. The vector method will provide us with new quantitative data about the local dynamics of cell movement, which is required in order to understand multicellular morphogenesis in *Dictyostelium*.

In contrast to measuring the movement of all cells in a tissue as in the case of the mound, it is also possible to follow the movement of individually marked cells. This can be achieved by choosing the lighting conditions such that the marked cells appear clearly distinct from the unlabelled cells that form a uniform background. Since under these conditions all grey values of unlabelled cells are similar, no spatial gradient can be detected and, correspondingly, no velocity will be detected for unlabelled cells (Fig. 3). Labelled cells can be easily tracked selectively. The movement track of each labelled cell will appear as a continuous track of pixels characterized by a velocity much higher than in surrounding pixels representing unlabelled cells. This is clearly demonstrated by displaying the average velocity of every pixel in the time series as a grey value (Fig. 3D,F). Distinct tracks of high velocity in the prespore zone can be seen. These represent the movement of individual neutral red-stained vacuoles in anterior-like cells. The neighbouring prespore cells contain too little structure for it to be detected under these lighting conditions. To investigate the rate of movement of all cells in a slug it will be necessary to change the lighting conditions to conditions similar to those used to analyse the rate of cell movement in mounds, where all cells contain some granular structure (for example, neutral red fluorescence found in all cells of a slug; author's unpublished observations).

The vector method detects moving objects most reliably if the objects move with an average speed of one pixel per frame (data not shown). Therefore it is necessary to choose the time interval between successive images to be analysed such that this condition is met. The sampling rate will therefore depend very much on the applied magnification. Our results show that it is possible to follow either distinctly labelled cells or unlabelled cells in tissues by choosing the appropiate optical conditions and/or labelling methods. The possibility of simultaneously displaying the velocity field and the video sequence from which the vector field was obtained, superimposed on each other, allows direct visual verification of the identified moving objects.

Another method based on a pixel correlation algorithm has been applied to early *Dictyostelium* aggregation and has been shown be able to measure direction and magnitude of cell movement (Steinbock et al., 1991). The drawback of this correlation method is that it requires lengthy calculations on mainframe computers. Our gradient method can be run on standard IBM-compatible computers or workstations with greatly reduced calculation time.

Understanding later morphogenesis in *Dictyostelium* as in other organisms requires a detailed analysis of cell movement. There are only very qualitative descriptions of the pattern of cell movement (Durston and Vork, 1979; Clark and Steck,

1979; Elliot et al., 1993). The vector velocity field method presented here allows the quantitative analysis of tissue and cell movement at all stages of *Dictyostelium* development. Our movement analysis shows that *Dictyostelium* development from the aggregation stage onwards is characterized by rotational cell movement. We find cells moving around a central core in aggregation centres, mounds (Fig. 2) and tips of slugs (Fig. 3). By analogy with early aggregation, it seems very likely that rotational cell movement is directed by counter-rotating chemotactic signals (Siegert and Weijer, 1992a; Steinbock et al.,1993).

Morphogenetic cell movements are of fundamental importance, not only during the development of *Dictyostelium* but also during embryonic pattern formation in vertebrates. Extensive morphogenetic movements occur during gastrulation and neurulation. The pixel-based velocity field analysis method might also prove to be useful in defining cellular movements of labelled and unlabelled cells in these more complex systems.

REFERENCES

Alcantara, F. and Monk M. (1974)**.** Signal propagation in the cellular slime mould *Dictyostelium discoideum*. *J. Gen. Microbiol.* **85**, 321-324.

Bonner, J., Hall D. and Suthers, H. (1989). Ammonia and thermotaxis - further evidence for a central role of ammonia in the directed cell mass movements of *Dictyostelium discoideum*. *Proc. Nat. Acad. Sci. USA* **86**, 2733-2736.

Clark, R. L. and Steck, T. L. (1979). Morphogenesis in *Dictyostelium*: An orbital hypothesis. *Science* **204**, 1163-1168.

Condeelis, J., Bresnick, A., Demma, M., Dharmawardhane, S., Eddy, R., Hall, A. L., Sauterer, R. and Warren, V. (1990). Mechanisms of amoeboid chemotaxis: an evaluation of the cortical expansion model. *Dev. Genet.* **11**, 333-340.

Durston, A. J. and Vork, F. (1979). A cinematographical study of the development of vitally stained *Dictyostelium discoideum*. *J. Cell Sci.* **36**, 261-279.

Elliot, S., Joss, G. H., Spudich, A. and Williams, K. L. (1993). Patterns in *Dictyostelium discoideum*: the role of myosin II in the transition from the unicellular to the multicellular phase. *J. Cell Sci.* **104**, 457-466.

Fisher, P., Merkl, R. and Gerisch, G. (1989). Quantitative analysis of cell motility and chemotaxis in *Dictyostelium discoideum* by using an image processing system and a novel chemotaxis chamber providing stationary chemical gradients. *J. Cell Biol.* **108**, 973-984.

Horn, B. K. P. and Schunk, B. G. (1981). Determining optical flow. *Artificial Intelligence* **17**, 185-203.

Kearney, J. K., Thompson, W. B. and Boley, D. L. (1987). Optical flow estimation: an error analysis of gradient based methods with local optimization. *IEEE Trans. Pattern Anal. Machine Intell.* **9**, 229-244.

Nomura, A., Miike, H. and Koga, K. (1991). Field theory approach for determining optical flow. *Pattern Recog. Lett.* **12**, 183-190.

Rubin, J. and Robertson, A. (1975). The tip of the *Dictyostelium discoideum* pseudoplasmodium as an organizer. *J. Embryol. Exp. Morph.* **33**, 1, 227-241.

Segall, J. (1988). Quantification of motility and area changes of Dictyostelium *discoideum* amoebas in response to chemoattractants. *J. Muscle Res. Cell Motil.* **9**, 481-490.

Segall, J. E. (1992). Behavioral responses of streamer-F Mutants of *Dictyostelium-discoideum* - effects of cyclic GMP on cell motility. *J. Cell Sci.* **101**, 589-597.

Siegert, F. and Weijer, C. J. (1991). Analysis of optical density wave propagation and cell movement in the cellular slime mould *Dictyostelium discoideum*. *Physica D* **49**, 224-232.

Siegert, F. and Weijer, C. J. (1992a). Three-dimensional scroll waves organize *Dictyostelium* slugs. *Proc. Nat. Acad. Sci. USA* **89**, 6433-6437.

Siegert, F. and Weijer, C. J. (1992b). The role of periodic signals in the morphogenesis of *Dictyostelium discoideum*. In *Oscillations and Morphogenesis* (ed. L. Rensing,), pp. 133-152. Marcel Dekker, New York.

Steinbock, O., Hashimoto, H. and Müller, S. C. (1991). Quantitative analysis of periodic chemotaxis in aggregation patterns of *Dictyostelium discoideum*. *Physica D* **49**, 233-239.

Steinbock, O., Siegert, F., Müller, S. C. and Weijer, C. J. (1993). Three-dimensional waves of excitation during *Dictyostelium* morphogenesis. *Proc. Nat. Acad. Sci. USA* **90**, 7332-7335.

Sussmann, M. M. (1987). Cultivation and synchronous morphogenesis of *Dictyostelium* under controlled experimental conditions. In *Dictyostelium discoideum: Molecular Approaches to Cell Biology.* Methods in Cell Biology, vol. 28 (ed. J. A. Spudich), pp. 9-29. Academic Press: New York.

Varnum, B., Edwards, K. B. and Soll, D. R. (1985). *Dictyostelium* amoebae alter motility differently in response to increasing versus decreasing temporal gradient of cAMP. *J. Cell Biol.* **101**, 1-5.

Wessels, D., Soll, D., Knecht, D., Loomis, W., Delozanne, A. and Spudich, J. (1988). Cell motility and chemotaxis in *Dictyostelium* amoebae lacking myosin heavy-chain. *Dev Biol.* **128**, 164-177.

Wessels, D., Murray, J. and Soll, D. R. (1992). Behavior of *Dictyostelium* amoebae is regulated promarely by the temporal dynamic of the natural cAMP wave. *Cell Motil. Cytoskel.* **23**, 145-156.